Article

# Ultrafast Electron Transfer Dynamics at NH/Cu(111) Interfaces: Determination of the Transient Tunneling Barrier

Julia Sta#hler, Michael Meyer, Daniela O. Kusmierek, Uwe Bovensiepen, and Martin Wolf

*J. Am. Chem. Soc.*, **2008**, 130 (27), 8797-8803 • DOI: 10.1021/ja801682u • Publication Date (Web): 14 June 2008



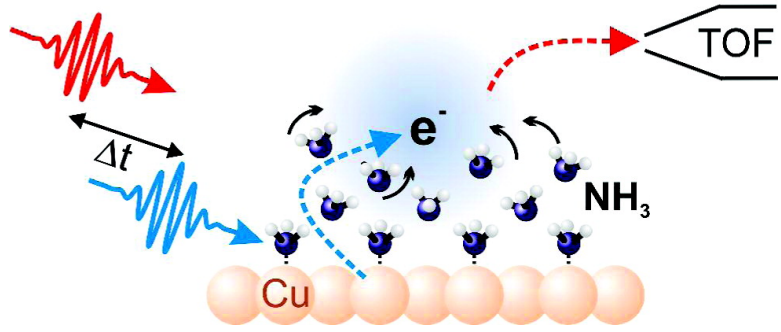


## More About This Article

Additional resources and features associated with this article are available within the HTML version:

- Supporting Information
- Links to the 3 articles that cite this article, as of the time of this article download
- Access to high resolution figures
- Links to articles and content related to this article
- Copyright permission to reproduce figures and/or text from this article

View the Full Text HTML

J|A|C|S
ARTICLES

Published on Web 06/14/2008

# Ultrafast Electron Transfer Dynamics at $NH_3$/Cu(111) Interfaces: Determination of the Transient Tunneling Barrier

Julia Stähler,* Michael Meyer, Daniela O. Kusmierek, Uwe Bovensiepen, and Martin Wolf

*Freie Universität Berlin, Fachbereich Physik, Arnimallee 14, 14195 Berlin, Germany*

Received March 6, 2008; E-mail: staehler@physik.fu-berlin.de

***Abstract:*** Electron transfer (ET) dynamics at molecule−metal interfaces plays a key role in various fields as surface photochemistry or the development of molecular electronic devices. The bare transfer process is often described in terms of tunneling through an interfacial barrier that depends on the distance of the excited electron to the metal substrate. However, a quantitative characterization of such potential barriers is still lacking. In the present time-resolved two-photon photoemission (2PPE) study of amorphous $NH_3$ layers on Cu(111) we show that photoinjection of electrons is followed by charge solvation leading to the formation of a transient potential barrier at the interface that determines the ET to the substrate. We demonstrate that the electrons are localized at the ammonia−vacuum interface and that the ET rate depends exponentially on the $NH_3$ layer thickness with inverse range parameters $\beta$ between 1.8 and 2.7 $nm^{-1}$. Systematic analysis of this time-resolved and layer thickness-dependent data finally enables the determination of the temporal evolution of the interfacial potential barrier using a simple model description. We find that the tunneling barrier forms after $\tau_E = 180$ fs and subsequently rises more than three times faster than the binding energy gain of the solvated electrons.

## 1. Introduction

As a basic phenomenon in nature, electron transfer (ET) is highly important for all disciplines of natural sciences. In fact, ET from a molecular donor to a molecular acceptor state is the simplest imaginable chemical reaction. Among others, ET plays a key role in the field of photochemistry where charge transfer from a metal substrate to adsorbed molecules can cause desorption or even chemical reactions at the interface.[1,2] Also, charge transfer from a molecular adlayer to a semiconducting substrate is the basic mechanism in dye-sensitized solar (Grätzel) cells.[3] Furthermore, electron transfer from metallic electrodes to organic systems is of vital significance for the prospering field of molecular electronics[4,5] where the length of the insulating buffer groups, which separate metallic ions from electrodes, determines the electronic coupling strength of the ion to the electrodes.[6]

The electron transfer process itself is described in terms of electron wave function overlap with the final state, which may be altered by a potential barrier that determines the transfer rate. *Without* such a tunneling barrier, the electronic wave function extends to the accepting state without being screened leading to strong coupling and fast electron transfer.[7,8] In many cases, however, charge transfer at interfaces is described by tunneling through a potential barrier.[1,9,10] For instance, desorption induced by electronic transitions (DIET) can be explained by electron transfer through an interfacial barrier.[1] However, as the shape of the potential barrier is not known, the excited state's lifetimes are not determined explicitly. Another difficulty for the description of electron transfer at molecule−metal interfaces occurs, if the character of the donating and accepting electronic state is modified by time-dependent variations of the molecular surrounding of the transferring electron. This effect is found, for example, in donor−bridge−acceptor systems in solution where molecular reorientations and bridge lengths strongly influence the ET rate.[11–13] These solvent-dependent charge transfer reactions are frequently described in terms of Marcus theory[14] where deformations of the molecular environment are condensed in a global reaction coordinate. Electron solvation occurs, however, not only in polar liquids[15,16] but also in gas phase

(1) Gadzuk, J. W. *Surf. Sci.* **1995**, *342*, 345.
(2) Zhu, X.-Y. *Annu. Rev. Phys. Chem.* **1994**, *45*, 113.
(3) O'Regan, B.; Grätzel, M. *Nature* **1991**, *353*, 737.
(4) Nitzan, A.; Ratner, M. A. *Science* **2003**, *300*, 1384.
(5) Zhu, X.-Y. *J. Phys. Chem. B* **2004**, *108*, 8778.
(6) Park, J.; Pasupathy, A. N.; Goldsmith, J. I.; Chang, C.; Yaish, Y.; Petta, J. R.; Rinkoski, M.; Sethna, J. P.; Abruna, H. D.; McCeuen, P. L.; Ralph, D. C. *Nature* **2002**, *417*, 722.
(7) Marinica, D. C.; Ramseyer, C.; Borisov, A. G.; Teillet-Billy, D.; Gauyacq, J. P.; Berthold, W.; Feulner, P.; Höfer, U. *Phys. Rev. Lett.* **1997**, *79*, 4645.
(8) Echenique, P. M.; Berndt, R.; Chulkov, E. V.; Fauster, Th.; Goldmann, A.; Höfer, U. *Surf. Sci. Rep* **2004**, *52*, 219.
(9) Gadzuk, J. W. *Surf. Sci.* **1974**, *43*, 44.
(10) Borisov, A. G.; Gauyacq, J. P.; Kazansky, A. K.; Chulkov, E. V.; Silkin, V. M.; Echenique, P. M. *Phys. Rev. Lett.* **2001**, *86*, 488.
(11) Nitzan, A. *Chemical Dynamics in Condensed Phases*; Oxford University Press: New York, 2006.
(12) Hayes, R. T.; Wasielewski, M. R.; Gosztola, D. *J. Am. Chem. Soc.* **2000**, *122*, 5563.
(13) Davis, W. B.; Ratner, M. A.; Wasielewski, M. R. *J. Am. Chem. Soc.* **2001**, *123*, 7877.
(14) Marcus, R. A. *J. Chem. Phys.* **1956**, *24*, 966.
(15) Lindner, J.; Unterreiner, A.-N.; Vöhringer, P. *Chem. Phys. Chem.* **2006**, *7*, 363.
(16) Migus, A.; Gauduel, Y.; Martin, J. L.; Antonetti, A. *Phys. Rev. Lett.* **1987**, *58*, 1559.

  

anion clusters.[17–19] Furthermore, such a transient molecular surrounding can also occur at molecule−metal or −semiconductor interfaces when excess electrons are injected into a polar environment as, for instance, water or ammonia: The electrons become localized in all three dimensions and are energetically stabilized (i.e., solvated) by reorientations of the surrounding molecular dipoles. The resulting wave function constriction[20–22] reduces the wave function overlap with the substrate and thus the electron transfer rate. The evolving molecular environment of the excess charge leads to changes of the electron potential including the tunneling barrier. As the time span of the actual ET process (i.e., the traversal time for tunneling) is assumed to be much shorter than the time scale of molecular reorientations,[23] charge transfer can be viewed as tunneling through a *transient* potential barrier that changes upon solvation on the time scale of solvent reorganization.

In the past, many studies focused on the investigation of the electron transfer and solvation dynamics at various molecule−metal interfaces, including water, alcohol, and alkane layers, and at molecule−semiconductor interfaces.[20,21,24–26] However, due to the complexity of the solvent−solute complex, neither exact theoretical description of the time-dependent tunneling barrier nor experimental determination of its temporal evolution has been achieved to date.[27] Here, we present a femtosecond time-resolved study of the electron transfer and solvation dynamics of excess electrons in amorphous $NH_3$ multilayers adsorbed on a Cu(111) single crystal surface using two-photon photoelectron (2PPE) spectroscopy. As will be discussed in section 3, we find two different regimes of electron dynamics, which are separated by a pronounced slowing of solvation and transfer at a time delay of $\tau_E = 180$ fs after photoexcitation. The initial femtosecond dynamics originate from solvated electrons in a precursor state $e_P$, crossing over to the fully solvated species $e_S$ exhibiting dynamics on picosecond timescales. This transition is well-reproduced by a three-level rate equation model that provides insight into the underlying processes. It will be shown that the excess electrons are localized at the ammonia vacuum interface, which enables the distance-dependent study of the electron population decay presented in section 3.4. By variation of the film thickness, we demonstrate that the population decay of the solvated electrons $e_S$ is mediated by tunneling through a potential barrier at the $NH_3$/Cu(111) interface. By a model description using parabolic potentials we aggregate the time- and distance-dependent data and quantify the temporal evolution of the interfacial tunneling barrier (section 4). This characterization of the transient potential, which is a measure for the screening reaction of the ammonia adlayer, allows for the explanation of the $e_S \rightarrow e_P$ transition of the interfacial electron dynamics: The precursor state $e_P$ is a laterally localized scattering state, which passes over into the further localized, solvated state $e_S$ due to the emergence of the interfacial tunneling barrier.

## 2. Experimental Section

After preparation of the Cu(111) single crystal surface following standard procedures,[28] amorphous[29] $NH_3$ layers are grown using a pinhole doser onto the substrate at 30 K under ultrahigh vacuum conditions ($p < 10^{-10}$ mbar). The coverage of $NH_3$ is determined using thermal desorption (TD) spectroscopy. The TD spectra exhibit three maxima, comparable to previous studies of $NH_3$/Ru(001).[30] Two peaks above 120 K correspond to the first and second monolayer (ML), and the signature of the zero-order desorption of the multilayer occurs for $T > 90$ K. The integrated TD intensities of the first and second ML are equal and are used as a mass equivalent.[31] The ammonia layer thickness $d$ is determined using the molecular density of solid $NH_3$. Here, it is assumed that the density of the $NH_3$ multilayers is comparable to the bulk value.[32] As the first two monolayers are probably thinner than the subsequent multilayers, this assumption may lead to an overestimation of the layer thickness by a constant value, which is accounted for by the given error bars.

Time-resolved 2PPE studies are performed using a commercial, regeneratively amplified Ti:Sa laser system providing 830 nm laser pulses at a repetition rate of 300 kHz. 20% of this output is frequency doubled ($h\nu_1 = 3.01$ eV) and used as the pump pulses (50 fs) for the 2PPE experiment as shown in the inset of Figure 1: Metal electrons from below the Fermi level $E_F$ are excited to unoccupied, bound states below the vacuum level $E_{vac}$. The subsequent electron dynamics in the ammonia adlayer are monitored by a time-delayed second laser pulse ($h\nu_2 = 2.41$ eV), which is generated in an optical parametric amplifier. It excites the electrons above the vacuum level $E_{vac}$, and their kinetic energy is analyzed using an electron time-of-flight (TOF) spectrometer. In the following, 2PPE spectra are plotted as a function of intermediate state energy with respect to the Fermi level: $E - E_F = E_{kin} + \Phi - h\nu_2$ (work function $\Phi$).

## 3. Electron Dynamics at the $NH_3$/Cu(111) Interface

The main panel of Figure 1 shows spectra of a 17 Å thick multilayer of $NH_3$/Cu(111) for a series of different time delays between 0 fs and 70 ps (right, logarithmic axis) as a function of intermediate state energy with respect to $E_F$ (bottom axis). Following excitation at $t = 0$ fs, the data exhibit a peak at $E_0 = 2.4$ eV above the metal Fermi level that shifts to lower energies with increasing pump−probe delay. As this observation is in line with other studies of

(17) Hertel, I. V.; Hüglin, C.; Nitsch, C.; Schulz, C. P. *Phys. Rev. Lett.* **1991**, *67*, 1767.
(18) Verlet, J. R. R.; Bragg, A. E.; Kammrath, A.; Cheshnovsky, O.; Neumark, D. M. *Science* **2005**, *307*, 93.
(19) Turi, L.; Sheu, W.-S.; Rossky, P. *Science* **2005**, *309*, 914.
(20) Bovensiepen, U.; Gahl, C.; Wolf, M. *J. Phys. Chem. B* **2003**, *107*, 165.
(21) Szymanski, P.; Garrett-Roe, S.; Harris, C. B. *Prog. Surf. Sci.* **2005**, *78*, 1.
(22) Gahl, C.; Bovensiepen, U.; Frischkorn, C.; Wolf, M. *Phys. Rev. Lett.* **2002**, *89*, 107402.
(23) Miller, R. J. D.; McLendon, G. L.; Nozik, A. J.; Schmickler, W.; Willig, F. *Surface Electron-Transfer Processes*; VCH: New York, 1995.
(24) Ge, N.-H.; Wong, C. M.; Harris, C. B. *Acc. Chem. Res.* **2000**, *33*, 111.
(25) Zhao, J.; Li, B.; Onda, K.; Feng, M.; Petek, H. *Chem. Rev.* **2006**, *106*, 4402.
(26) Li, B.; Zhao, J.; Jordan, K. D.; Yang, J.; Petek, H. *Science* **2006**, *311*, 1436.
(27) Mixed quantum-classical molecular dynamics simulations have recently been used to investigate the localization and stabilization dynamics at various water/air interfaces [Madarász, Á.; Rossky, P. J.; Turi, L. *J. Chem. Phys.* **2007**, *126*, 234707]. The observed localization and stabilization dynamics with a concomitant spatial constriction might have implications for similar systems like the ammonia surfaces investigated here.
(28) Knoesel, E.; Hotzel, A.; Wolf, M. *Phys. Rev. B: Condens. Matter* **1998**, *57*, 12812.
(29) Crystallization of $NH_3$/Cu(111) occurs at 100 K as will be shown in a future publication.
(30) Benndorf, C.; Madey, T. E. *Surf. Sci.* **1983**, *135*, 164.
(31) The coverage of 1 ML corresponds to 0.25 $NH_3$ molecules per Cu atom. Baumgärtel, P.; Lindsay, R.; Giessel, T.; Schaff, O.; Bradshaw, A. M. *J. Phys. Chem.* **2000**, *104*, 3044.
(32) Fortes, A. D.; Brodholt, J. P.; Wood, I. G.; Vočadlo, L. *J. Chem. Phys.* **2003**, *118*, 5987.

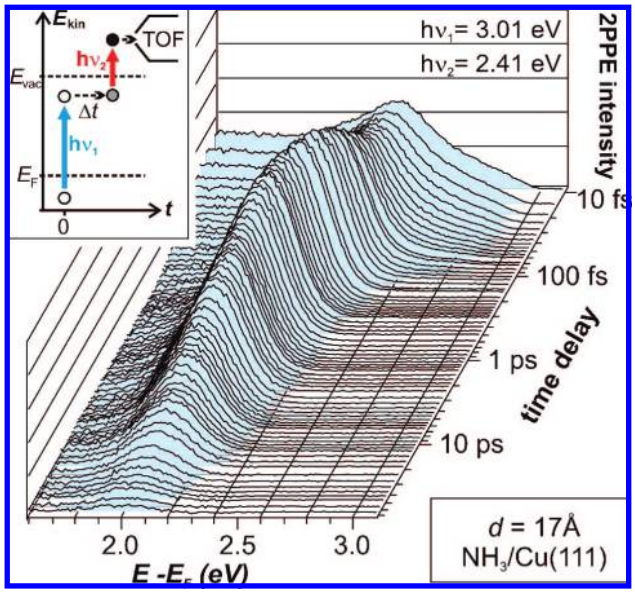


***Figure 1.*** Time-resolved 2PPE of a 17 Å thick amorphous $NH_3$ film on Cu(111) at 30 K for different time delays up to 70 ps. The signal below 2.5 eV is attributed to solvated electrons in the adlayer that are stabilized by the surrounding polar molecules. Inset: 2PPE scheme. Metal electrons are excited by a first femtosecond-laser pulse ($h\nu_1$) into unoccupied, bound states. The intermediate state's dynamics are monitored by a second, time-delayed laser pulse ($h\nu_2$) that excites electrons above the vacuum level. Their kinetic energy is analyzed using a time-of-flight (TOF) spectrometer.

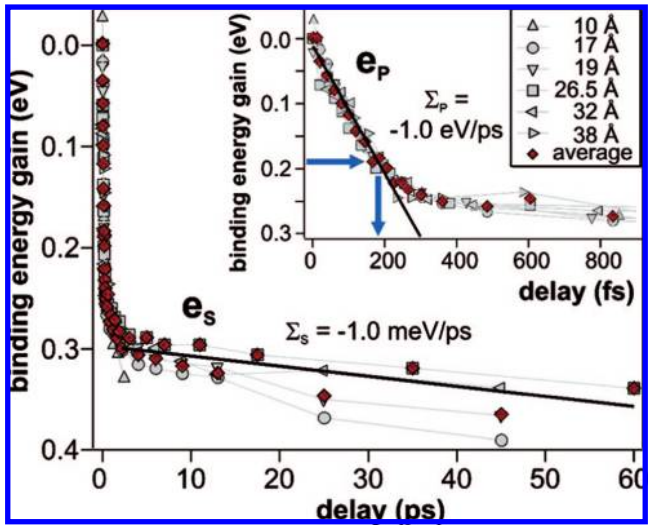


***Figure 2.*** Binding energy gain of the peak maximum of the solvated electron distribution as a function of time delay for various $NH_3$ layer thicknesses (gray) and the average evolution (red) with respect to the initial energy of the excess electrons at $t = 0$ fs. For $t < 200$ fs, the peak maximum shifts with a rate of 1 eV/ps towards the Fermi level (inset). After 200 fs, the energy shift starts to slow down to 1 meV/ps.

polar molecule−solid interfaces,[33,26,20] we attribute this feature to electron solvation in the adlayer caused by rearrangement of surrounding $NH_3$ molecules that accommodate the excess charge.

**3.1. Binding Energy Gain.** Figure 2 depicts the time evolution of the binding energy gain $E_B = E_0 - E$, which

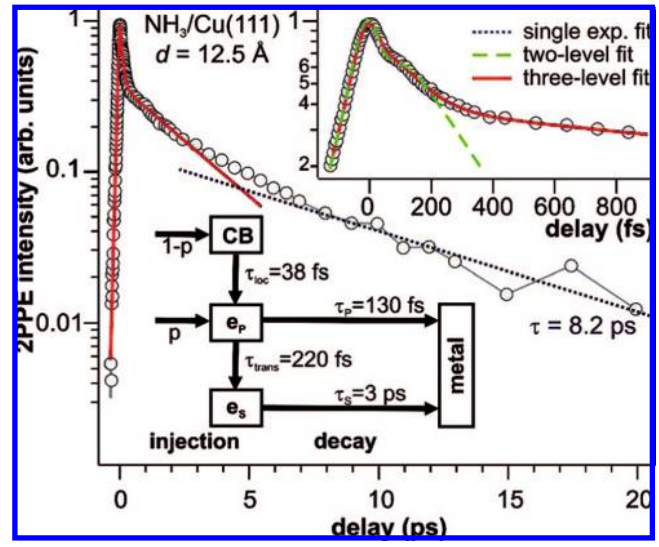


***Figure 3.*** Electron population dynamics. The solvated electron population transient (open symbols) is well fitted with a single exponential for $t = 10-20$ fs (blue line); green and red curves based on the two- and three-level rate equation approaches. The flowchart represents the latter, reproducing the data up to 3 ps.

characterizes the average energy shift of the solvated electron distribution with respect to its initial energy at $t = 0$ fs, for various layer thicknesses $d$ (gray) and the average evolution (red). The inset depicts a linear fit to the data (black line) showing that the peak maximum shifts initially ($t < 200$ fs) toward the Fermi level with a rate of $\Sigma_P = -1.0$ eV/ps. After 200 fs the rate is significantly reduced and reaches the value $\Sigma_S = -1$ meV/ps in the picosecond time regime (main panel). The pronounced difference between these two rates suggests two different species of interfacial electrons that we term $e_P$ and $e_S$ in the following.

**3.2. Population Dynamics.** The main panel of Figure 3 shows the transient 2PPE intensity of the solvated electron distribution as a function of time delay (open circles).[34] For late delays (>3 ps), the population decay is very well fitted by a single exponential decay (dotted line) with a decay constant of 8.2 (±1.2) ps. As apparent from Figure 1, the time-dependent change of the intensity of the solvated electron feature is more complicated in the femtosecond time regime than at picosecond time delays, as the processes of charge injection and electron population decay occur simultaneously. Thus, a more sophisticated analysis is required for $t < 1$ ps. In a first attempt, the data were fitted using a two-level rate equation accounting for the delocalized conduction band and one localized solvated electron state. The least-squares fit is given in the inset of Figure 3 by the green dashed curve. The delayed intensity rise at 100 fs and the subsequent population transient are reproduced up to ~200 fs. However, at larger delays the measured population decay slows drastically, similar to the shift of the peak maximum observed in Figure 2, a behavior that cannot be reproduced by the two-level rate equation approach. To quantitatively analyze this effect, the rate equation model is extended to three levels—the conduction band, a precursor state $e_P$, and the solvated species $e_S$—as illustrated by the flowchart in Figure 3. For the excitation pathway, we consider electrons that are excited to the conduction band (CB) with the probability (1 −

(33) Miller, A. D.; Bezel, I.; Gaffney, K. J.; Garret-Roe, S.; Liu, S. H.; Szymanski, P.; Harris, C. B. *Science* **2002**, *297*, 1163.

(34) The transient population is achieved by integrating the 2PPE intensity over the energy window of $E - E_F = 1.4$ to 2.7 eV.

$p$) and electrons that are excited directly to the solvated electron state $e_S$ with the probability $p$. The localization at favorable sites in the adlayer, i.e., the transition from the conduction band to the presolvated species, is described by the localization rate $\Gamma_{loc}$. After charge injection, the $e_P$ electrons may either decay back to the Cu(111) substrate with the probability $\Gamma_P = \tau_P^{-1}$ or cross over to species $e_S$ with the transition probability $\Gamma_{trans} = \tau_{trans}^{-1}$. The transfer probability of $e_S$ electrons back to the metal is $\Gamma_S = \tau_S^{-1}$. The solution of the resulting rate equation system (see Supporting Information) leads to the following expressions for the electron population dynamics in the precursor and solved state, respectively:

$$n_P(t) = \underbrace{\frac{p(\Gamma_P + \Gamma_{trans}) - \Gamma_{loc}}{\Gamma_P + \Gamma_{trans} - \Gamma_{loc}}}_{A} \cdot \exp\left[-(\Gamma_P + \Gamma_{trans})\cdot t\right] + \underbrace{\frac{(1-p)\Gamma_{loc}}{\Gamma_P + \Gamma_{trans} - \Gamma_{loc}}}_{B} \cdot \exp\left[-\Gamma_{loc}\cdot t\right] \quad (1a)$$

$$n_S(t) = \frac{\Gamma_{trans}}{\Gamma_S - (\Gamma_P + \Gamma_{trans})} \cdot A \cdot \left\{e^{-(\Gamma_P + \Gamma_{trans})t} - e^{-\Gamma_S t}\right\} + \frac{\Gamma_{trans}}{\Gamma_S - \Gamma_{loc}} \cdot B \cdot \left\{e^{-\Gamma_{loc} t} - e^{-\Gamma_S t}\right\} \quad (1b)$$

The population transient of the precursor species $e_P$ (eq 1a) is determined by the population increase due to localization from the CB with the probability $\Gamma_{loc} = \tau_{loc}^{-1}$ and the two decay channels resulting from electron transfer to the metal with the rate $\Gamma_P$ and transition to species $e_S$ with the probability $\Gamma_{trans}$. The population of the solvated species $e_S$ (eq 1b) on the other hand increases due to electrons originating from $e_P$ and decreases due to electron decay back to the metal substrate. The sum of these population transients was fitted to the data after convolving with the laser pulses' envelope.[35] As apparent by the solid curves in Figure 3, the least-squares fit nicely reproduces the population trace up to 3 ps. It is noteworthy that the fit function does not include any further scaling factors. For given initial conditions, all amplitudes consistently result from the rate constants as described by eqs 1a and 1b, supporting the three-level rate equation model. Fitting always leads to a vanishing probability $p$, showing that charge injection occurs *indirectly* via the CB continuum.[36] This result can be rationalized by considering a wave function overlap between delocalized CB electrons and the trapping site. Further results from the fit for the 12.5 Å thick $NH_3$ adlayer are given in the flowchart of Figure 3. The time constants $\tau_{loc}$, $\tau_P$, and $\tau_{trans}$ vary only weakly with ammonia layer thickness: Averaging these values for coverages between 12.5 and 32 Å shows that the excess electrons localize from the conduction band to the precursor state $e_P$ with a time constant of $\tau_{loc} = 36(6)$ fs. The transition from $e_P$ to the solvated species $e_S$ occurs within $\tau_{trans} = 180(40)$ fs. In parallel with the localization and the $e_P \rightarrow e_S$ transition, the electrons in the precursor state $e_P$ decay back to the metal substrate with the characteristic time $\tau_P = 140(20)$ fs. The lifetimes of species $e_S$ strongly vary with $NH_3$ layer thickness and will be discussed in section 3.4.

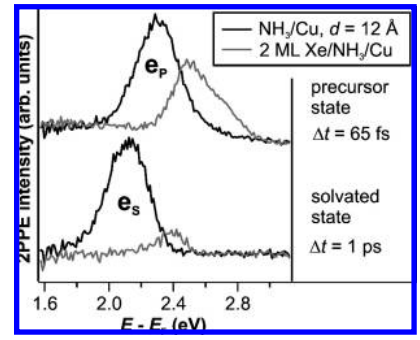


***Figure 4.*** Xenon titration experiment. The solvated electron peak of both species, precursor state $e_P$ (top) and solvated state $e_S$ (bottom), shifts to higher energies upon Xe adsorption on top of the $NH_3$ layer showing that the electrons are localized at the ammonia−vacuum interface.

In line with the analysis above, the electron transfer and solvation dynamics at the $NH_3$/Cu(111) interface can be summarized as follows: We have shown that relaxation of photoexcited electrons at the $NH_3$/Cu(111) interface by electron transfer and solvation occurs via two different species of interfacial electrons, $e_P$ and $e_S$. Angle-resolved experiments (not shown) unveil that both species are laterally localized states. The species $e_P$ exhibits transfer and stabilization dynamics on femtosecond timescales. The transition from this precursor state to the second species $e_S$ occurs with a time constant of 180 fs, which is consistent with the slowing of the energy shift in Figure 2 upon the $e_P \rightarrow e_S$ transition. After this abrupt conversion, the solvated species $e_S$ exhibits picosecond dynamics in electron transfer and solvation. As shown in Figure 3, the electron decay at these late time delays slows *continuously* with increasing time delay. This deceleration occurs steadily, in contrast to the abrupt transition from $e_P$ to $e_S$. The proceeding solvation leads to an enhanced screening of the excess charge from the metal and therefore to a gradual slowing of the electron transfer, a behavior that is already known for ice−metal interfaces.[22,37]

**3.3. Solvation Site.** In addition to the time-resolved investigations of the interfacial electron dynamics, we performed a xenon overlayer experiment of the solvated electrons to unveil their binding site.[38] It is known from previous work that, in the case of surface solvation, adsorption of one or more monolayers of Xe significantly affects the electron transfer and solvation dynamics: The charge cloud of the surface-solvated species interacts directly with the Xe atoms, leading to polarization of the rare gas and to energetic shifts of the solvated electron peak by several 100 meV.[38] In the case of solvation in the bulk of the adlayer, the solvated electron is screened by the surrounding solvent molecules so that only minor changes of the photoelectron spectra are observed.[39] Figure 4 depicts the Xe titration experiment for $d = 12$ Å $NH_3$ on Cu(111). 2PPE spectra before

(35) To take into account the time-dependent background of hot electrons, which are excited by the visible light, an additional exponential decay to negative delays was added to the fit function.

(36) This result is confirmed by the data in Figure 1. If direct, resonant excitation of the solvated electrons at $E - E_F = 2.4$ eV was possible, such electrons would be probed by UV photons ($h\nu = 3.0$ eV) and should lead to a "twin" peak of the solvated electrons in the experiment at $t = 0$ fs and $E - E_F = 3$ eV. The absence of such a signal in Figure 1 shows that excitation cannot occur resonantly.

(37) Stähler, J.; Bovensiepen, U.; Gahl, C.; Wolf, M. *J. Phys. Chem.* **2006**, *110*, 9637.

(38) Stähler, J.; Mehlhorn, M.; Bovensiepen, U.; Meyer, M.; Kusmierek, D. O.; Morgenstern, K.; Wolf, M. *Phys. Rev. Lett.* **2007**, *98*, 206105. presents a xenon-titration experiment of surface-solvated electrons at amorphous ice clusters on Cu(111).

(39) Stähler, J. PhD thesis, *Freezing Hot Electrons - Electron Transfer and Solvation Dynamics at D2O and NH3-Metal Interfaces*, Freie Universität Berlin, Fachbereich Physik, 2007 (http://www.diss.fu-berlin.de/2007/479/).

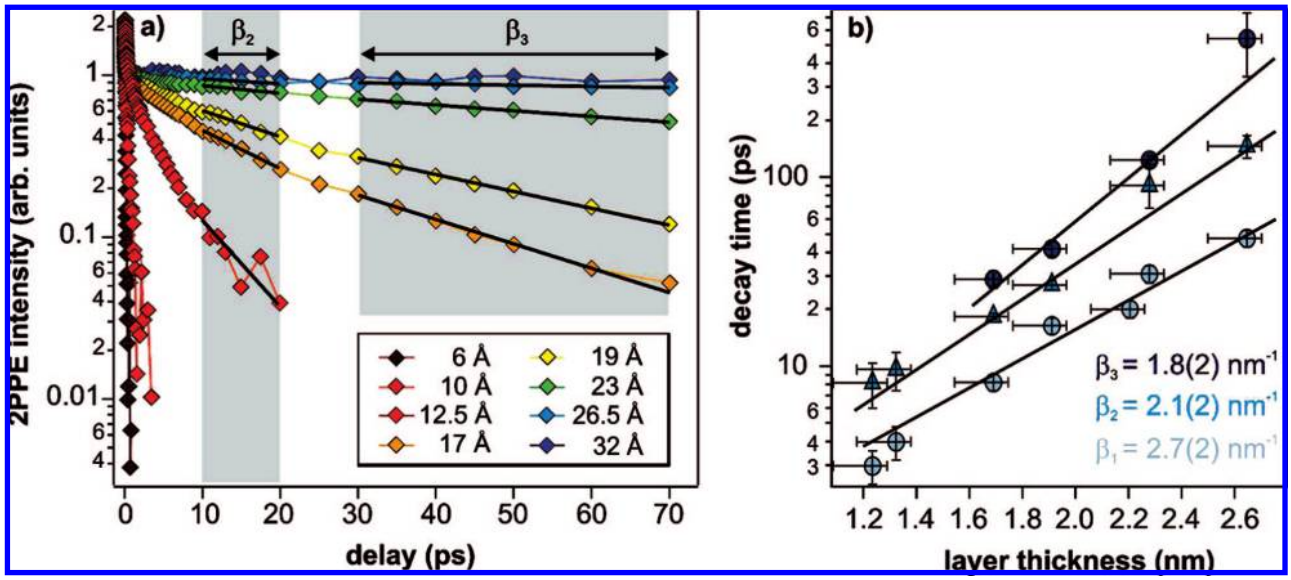


***Figure 5.*** (a) Normalized population transients for different layer thicknesses of $NH_3$/Cu(111). Black lines are single exponential fits to the data for decay time quantification. (b) Thickness dependence of population decay times extracted at early (<3 ps, light blue), medium (10−20 ps, blue), and late delays (30−70 ps, dark blue) as indicated in panel a by the black lines. Asymmetric error bars result from the layer thickness determination.

Xe adsorption (black curves) at time delays of 65 fs (top) and 1 ps (bottom) represent the precursor state $e_P$ and the solvated species $e_S$, respectively. As apparent from the figure, adsorption of 2 ML xenon on top of the ammonia layers leads to significant changes of the photoelectron spectra: Upon Xe titration (gray curves), the peak maxima shift by 200(20) meV for the precursor state and 270(20) meV for the solvated electrons. These significant changes of binding energies for both species unveil that $e_P$ and $e_S$ are localized in the surface region of the $NH_3$ layer.

Having characterized the electron dynamics at the $NH_3$/Cu(111) interface and having unveiled the binding site of $e_P$ and $e_S$, the next section presents the coverage dependence of the electron dynamics at the $NH_3$/Cu(111) interface. Such distance-dependent ET reactions also occur for donor−bridge−acceptor systems in solution where the bridge length is determined by the number of $\sigma$-bonds of the molecular spacer group.[11] The following key experiment shows that electron transfer is mediated by tunneling through an interfacial potential barrier and finally enables the quantitative characterization of the transient tunneling barriers in section 4.

**3.4. Distance-Dependent Tunneling.** Figure 5a depicts population transients of several layer thicknesses between 6 and 32 Å of amorphous $NH_3$ on Cu(111). The electron population traces exhibit a pronounced thickness dependence: The population decay rate slows significantly down with increasing coverage. While the decay occurs on femtosecond timescales for a 6 Å (dark red) thick film, the 2PPE intensity remains constant up to 70 ps for coverages of more than 26.5 Å (blue). The corresponding decay times are quantitatively analyzed by single exponential fits (black lines) for late and medium delay times (shaded areas) and by the rate equation approach developed above for delay times < 3 ps. The resulting three data sets, which reflect the coverage-dependent electron decay times in three different, exemplary stages of solvation, are given in Figure 5b. For any layer thickness, the decay times at early delay times (light blue, $t$ < 3 ps) are smaller than the ones at medium (blue, $t$ = 10−20 ps) and late delay times (dark blue, $t$ = 30−70 ps). This reflects that the excess charge is continuously screened from the substrate during electron solvation leading to a decreasing decay probability. Most substantial is that all three data sets of electron transfer times exhibit an *exponential* dependence on layer thickness. This remarkable observation combined with the finding that the electrons are located at the ammonia−vacuum interface demonstrates that electron transfer proceeds by tunneling through a potential barrier which depends on the layer thickness. As the tunneling probabilities depend exponentially on $d$, the electron lifetime is proportional to

$$\tau(d) \propto \exp[\beta \cdot d] \tag{2}$$

where $\beta$ is the *inverse range parameter* in the respective state of solvation. This characteristic quantity is a measure for the influence of the effective electron mass and barrier height on the tunneling probability.[11] Single exponential fits (Figure 5b, black lines) yield $\beta_1 = 1.8$ nm$^{-1}$, $\beta_2 = 2.1$ nm$^{-1}$, and $\beta_3 = 2.7$ nm$^{-1}$ for the three data sets. These increasing $\beta$-parameters illustrate that the tunneling barrier increases during the stabilization process, as they correspond to the different "snap shots" of electron solvation at 2(1), 15(5), and 50(20) ps, respectively. Moreover, the parameters can be correlated to the binding energy gain $E_B(t)$ of the solvated electron distribution using the time-dependent energy shift shown in Figure 2: $\beta_1 = \beta(0.29$ eV), $\beta_2 = \beta(0.31$ eV), and $\beta_3 = \beta(0.35$ eV). It is noteworthy that these values contain the time- and coverage-dependent evolution of the transient potential barrier.[12] Their physical significance will be discussed in the following section and will be used to quantify the temporal evolution of the interfacial tunneling barrier.

## 4. Determination of Transient Potential Barriers

The inverse range parameters $\beta_i$ characterize the tunneling barrier in the respective transient state of solvation. In the simplest case of a rectangular potential barrier (Figure 6a), the $\beta$-parameter is determined by the barrier height $V_0$ and the energy $E$ of the tunneling electron:

$$\beta(E) = \frac{2}{\hbar}\sqrt{2m(V_0 - E)} \tag{3}$$

Figure 6a illustrates that the description of the potential by a rectangle is insufficient, as the width of the barrier cannot be

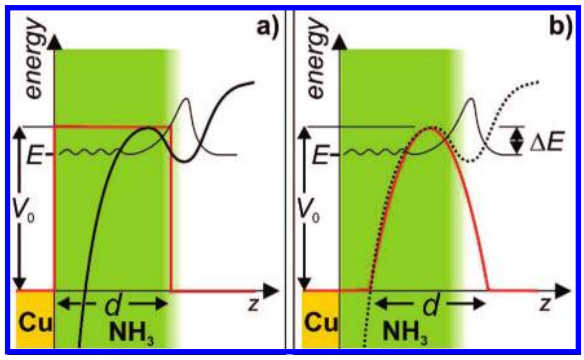


***Figure 6.*** Model potentials for the interfacial tunneling barrier. (a) The rectangular barrier is not a good approximation, as it does not become narrower at its maximum. (b) The parabolic potential.

set equal with the layer thickness and as it has a constant width at all energies. Both shortcomings lead to a significant underestimation of the tunneling probabilities, which depend on the barrier width at all energies larger than $E$. This is different when assuming a parabolic barrier as depicted in Figure 6b, as it accounts for the steady narrowing at the top of the barrier. Calculation of the $\beta$-parameter for such parabolic potential yields[40]

$$\beta(E) = \frac{\pi}{2\hbar}\sqrt{2mV_0(E)}\left(1 - \frac{E}{V_0(E)}\right) \quad (4)$$

Here, the potential $V(z) = V_0 - az^2$ is used with the barrier maximum at $V_0$ and, as a first approach, with a curvature $a = 4V_0/d^2$, yielding a potential barrier that is as wide as the layer thickness $d$ right at the Fermi level of the system (cf. Figure 6b). The energy difference between the potential barrier maximum and the energy of the solvated electrons, which we term *relative barrier height* $\Delta E(E) = V_0(E) - E$, changes with ongoing solvation. Such variation

$$\frac{\partial \Delta E(E)}{\partial E} \equiv \kappa \quad (5)$$

can result from two different mechanisms: (i) The solvated electron continuously gains binding energy. Even if the barrier remained constant, $\Delta E$ would increase ($\kappa = 1$). (ii) The molecular rearrangement leading to the binding energy gain mentioned above may lead to an enhanced screening of the electron from the metal and thus to an *additional* increase of the barrier height ($\kappa > 1$).

Quantification of this evolution of the potential barrier with proceeding solvation is achieved by extracting the relative barrier height $\Delta E$ from eq 4:

$$\Delta E(E) = V_0(E) - E = \frac{\hbar \cdot \beta(E)}{\pi \cdot m}\left\{\frac{\hbar \cdot \beta(E)}{\pi} + \sqrt{\left(\frac{\hbar \cdot \beta(E)}{\pi}\right)^2 + 2mE}\right\} \quad (6)$$

The energy dependence of the three experimentally determined $\beta_i$ allows for the calculation of the corresponding tunneling barrier heights using eq 6. These are depicted in Figure 7a (solid markers) as a function of binding energy gain $E_B$ of the solvated electron distribution enabling the determination of $\kappa$:[41] A linear fit to the data results in an increase of the relative barrier height by $\kappa = 3.6$; i.e., the barrier enhancement is much

(40) Schwabl, F. *Quantum Mechanics*; Springer: Berlin, 1992.
(41) For this calculation the free electron mass was assumed.

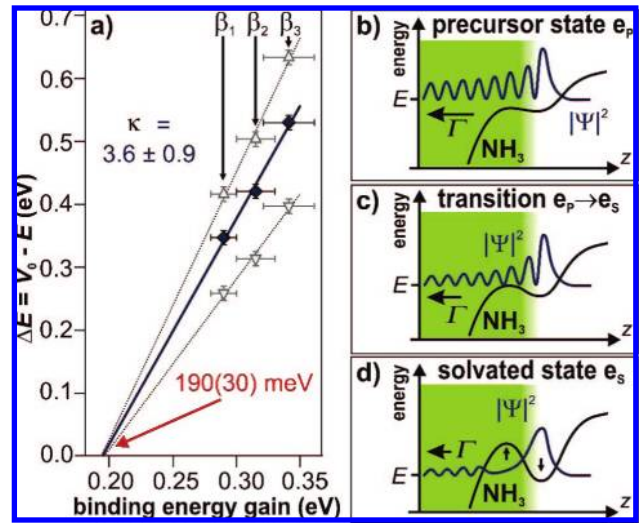


***Figure 7.*** Determination of tunneling barriers. (a) Relative barrier height as a function of binding energy gain of the solvated electrons for three different parabola curvatures. Linear extrapolation of the barrier evolution leads to a vanishing of the barrier at the same binding energy (red arrow) for all data sets. (b–d) Schematic description of the $e_S \rightarrow e_P$ transition: (b) The precursor state $e_P$ is above the potential barrier maximum and therefore a scattering state. (c) The transition to the solvated species occurs when the electron energy reaches the potential barrier maximum. (d) Electron transfer from the solvated state $e_S$ is characterized by tunneling through the potential barrier.

stronger than the mere binding energy gain of the solvated electrons due to increased screening of the excess electron by the surrounding polar molecules: For each 10 meV binding energy gain of the solvated electrons, the barrier increases by 36 meV (i.e., additional 26 meV), illustrating the impact of electron solvation on the charge transfer.

Extrapolation of the linear dependence of barrier height to $\Delta E = 0$ eV (blue line) shows that the barrier is zero for electrons that gained $E_E = 190(30)$ meV of binding energy after photoexcitation. Thus, the above analysis enables the observation of the *emergence* of the tunneling barrier: For binding energies $E_B < E_E$ there is a vanishing barrier height, while it significantly increases for $E_B > E_E$. Remarkably, this result does not depend on the curvature $a$ of the parabolic potential, as demonstrated by the dotted lines in Figure 7a, which result from parabola curvatures changed by ±40%. These data sets also provide a conservatively estimated upper limit for the error bar of the barrier enhancement factor of $\kappa = 3.6 \pm 0.9$.

The binding energy $E_B(t)$ of the solvated electron distribution is a function of delay time. Therefore, the energy $E_E$, at which the barrier emerges, can be translated to a characteristic time $\tau_E = 180(50)$ fs as illustrated by the blue arrows in the inset of Figure 2. At earlier delay times, the energy of the interfacial electrons is above the potential barrier maximum as sketched in Figure 7b. The electronic wave function is comparably delocalized in the direction normal to the surface, extending through the adsorbate layer into the Cu(111) substrate: In this regime the electron wave function resembles a scattering state. After $\tau_E = 180$ fs, when the barrier maximum and interfacial electron have the same energy (Figure 7c), the transition to the tunneling state occurs. At larger delays (Figure 7d) the electronic wave function is separated from the metal substrate by a potential barrier that reduces the transfer probability as it continuously rises and therefore increasingly screens the excess charge as indicated by the arrows.

Remarkably, this characteristic time of $\tau_E = 180(50)$ fs for the transition from the scattering to the tunneling state coincides with the transition time $\tau_{trans} = 180(40)$ fs obtained above using the rate equation analysis of the population dynamics in section 3.2. It characterizes the transition from the precursor state $e_P$ to the solvated species $e_S$. This coincidence of the two independently achieved time constants strongly supports both the rate equation analysis (assuming two different species of interfacial electrons) *and* the model description of the tunneling potential by transient parabolic potential barriers. Moreover, it allows for the assignment of the precursor state $e_P$ to be of the scattering type as depicted in Figure 7b in contrast to the solvated state $e_S$ which has tunneling character (Figure 7d). In other words, the origin of the $e_P \rightarrow e_S$ transition is unveiled: Initially, after charge injection of metal electrons via the ammonia CB, the excess electrons localize in the precursor state $e_P$, which extends through the adsorbate layer into the metal substrate. The continuous solvation of the precursor−electron leads to further (lateral and normal) localization, which is accompanied by the emergence of the tunneling barrier: The barrier emerges and finally screens the electronic wave function of the solvated electron from the metal substrate. Henceforth, electron transfer is mediated by tunneling through the dynamically evolving potential barrier.

## 5. Summary and Conclusions

Electron transfer and solvation dynamics at $NH_3$/Cu(111) interfaces are investigated as a function of coverage using femtosecond time-resolved 2PPE spectroscopy and Xe titration experiments. We find two different species of interfacial electrons, a precursor state $e_P$ and the solvated species $e_S$, which are both localized at the ammonia−vacuum interface. The precursor $e_P$ is characterized by femtosecond electron transfer and solvation dynamics and the solvated state $e_S$ by dynamics on picosecond timescales that depend exponentially on the ammonia layer thickness. The comparably abrupt transition is analyzed by an empirical rate equation approach and a model description of the interfacial potential by transient parabolic tunneling barriers. Both independent approaches yield a characteristic time of 180 fs for the $e_P \rightarrow e_S$ transition, showing the adequacy of the model description of the tunneling barriers by parabolic potentials. It is demonstrated that the transition from the precursor to solvated state is due to the emergence of the tunneling barrier: While the precursor $e_P$ is a scattering state, which extends through the adlayer into the metal substrate without passing through a potential barrier, the solvated state $e_S$ is of tunneling character; i.e., the electronic wave function overlap with the metal is strongly reduced because of the presence of a potential barrier that screens the electrons from the metal.

Our work comprises the first quantitative determination of transient potential barriers at molecule−metal interfaces. In particular, the presented results demonstrate that the plain assumption of parabolic potentials is not only consistent with the independent rate equation analysis but also capable of explaining fairly complex electron dynamics as observed in the present article. These results are of general interest for various fields where interfacial charge transfer occurs, as the transient potential energy landscape is quantitatively monitored during dynamic changes due to electron−molecule interaction.

**Acknowledgment.** We thank S. Fischer and C. Gahl for fruitful discussions and acknowledge funding by the Deutsche Forschungsgemeinschaft through Sfb 658, the German Israeli Foundation, and the International Max Planck Research School for Complex Surfaces in Material Science.

**Supporting Information Available:** Derivations of eqs 1a and 1b. This material is available free of charge via the Internet at http://pubs.acs.org.

JA801682U